Composites Science and Technology 68 (2008) 2092–2102

Contents lists available at ScienceDirect

Composites Science and Technology

journal homepage: www.elsevier.com/locate/compscitech

# Generation of random distribution of fibres in long-fibre reinforced composites

A.R. Melro [a], P.P. Camanho [a,*], S.T. Pinho [b]

[a] DEMEGI, Faculdade de Engenharia, Universidade do Porto, Rua Dr. Roberto Frias, 4200-465 Porto, Portugal
[b] Department of Aeronautics, Imperial College London, South Kensington Campus SW7 2AZ, UK

ARTICLE INFO

*Article history:*
Received 10 January 2008
Received in revised form 14 March 2008
Accepted 17 March 2008
Available online 28 March 2008

*Keywords:*
B. Microstructure
C. Statistics
C. Elastic properties

ABSTRACT

This paper presents a new model to the generation of the transversal cross-section of long-fibre reinforced composites with high fibre volume fraction, characterised by a random distribution of the reinforcements. This stochastic nature has a significant influence on the microscopical distribution of stresses and strains and therefore on damage initiation and subsequent propagation. A simple and fast algorithm to model the random distribution of fibres is proposed. The algorithm is statistically characterised and the results show that it is capable of capturing the random distribution typical of these materials even for high fibre volume fractions. Predictions of some effective properties of the lamina through finite element analyses is performed and a good agreement with experimental results is found.



## 1. Introduction

The increasing demand from the industry to use composite materials requires cost-effective techniques capable to accurately predict the elastic properties of composites from the properties of their constituents. Traditionally, a full experimental campaign is conducted to fully characterise a given mixture of constituents, for a given volume fraction of reinforcement. This requires a considerable amount of human, financial and time resources.

The current trend of work in micromechanics addresses the industry's requirement to decrease the dependence on experimental work, and complement it with new numerical and/or analytical processes capable of providing quickly and efficiently the same information. A highly attractive process to simulate the real mechanical behaviour of the composite is through finite element analysis. For that, a Representative Volume Element (RVE) of the material needs to be defined and an equivalent random distribution of fibres generated.

The first issue concerning the use of a RVE is its dimension. The RVE cannot be too large as this would endanger the possibility to numerically analyse it; however, it cannot be too small either as it could not be representative of the composite material. Shan and Gokhale [1] studied the microstructure of a ceramic matrix composite with random distribution and size of the reinforcement, concluding that a window of approximately 40× the average fibre radius for a volume fraction of 35% represented both geometrically and mechanically the constitutive behaviour of the material. Trias et al. [2] demonstrated that for long-fibre reinforced composites made of carbon fibre and epoxy matrix a value of 50× the fibre radius should be used.

The second issue involving the use of an RVE is the spatial arrangement of reinforcements which normally is not periodic and is highly dependent upon the manufacturing process. Brockenbrough et al. [3] have shown that in the plastic regime, the transverse deformation cannot be predicted correctly if a periodic fibre distribution is used. Pyrz [4,6] observed that the transverse constitutive behaviour of polymer matrix composites is a function of the spatial arrangement of the reinforcements. Matsuda et al. [5] compared the elastic–viscoelastic behaviour of long-fibre reinforced laminates subjected to in-plane tensile loading using homogenization theory, and concluded that the spatial distribution of the reinforcements in the RVE does not affect the macroscopic response of laminates, but it significantly affects the microscopic stress distribution. It is thus important to consider transverse randomness of fibre distribution for studying the onset and evolution of damage in the matrix.

The Poisson point distribution [6] provides a statistical distribution of points inside a given area. The probability of finding a point in any coordinate of the area of interest is exactly the same. However, this method deals with points of zero radial dimension and does not guarantee non-overlapping fibres. The hard-core model [6] overcomes this difficulty by considering that points are centres of fibres and the probability of finding a point at a distance to another point less or equal the fibre diameter is zero. The only setback about this process is that it hardly generates distributions with fibre volume fractions greater than 50% [7]. Feder [8] demonstrated that the Random Sequential Adsorption (RSA) [9] algorithm used, for example, in particle deposition studies [10] has a jamming limit of 54.7%, thus not suitable for high fractions of fibre

* Corresponding author. Tel.: +351 225081753; fax: +351 225081584.
*E-mail address:* pcamanho@fe.up.pt (P.P. Camanho).

0266-3538/$ - see front matter © 2008 Elsevier Ltd. All rights reserved.
doi:10.1016/j.compscitech.2008.03.013

volume. Wongsto and Li [11] proposed an algorithm that can generate a fibre distribution with a high fibre volume fraction by disturbing an initially hexagonal periodic array. However, this algorithm was not statistically analysed. Jodrey and Tory [12] provide an algorithm to generate a random distribution of spheres in 3D. The same procedure can be used in 2D for a distribution of disks, but the authors advise the final configuration may not be random. Oh et al. [13] proposed a method based on the hard-core model, whose implementation by the authors resulted in a maximum of 50% of fibre volume fraction, which clearly is too low a value for the type of composite materials under investigation in this paper. Buryachenko et al. [7] provide a good review of some numerical methods and their jamming limits as well as experimental limits for sphere and/or disk arrangements. Digital image analysis [14] provides a perfect replica of the transverse section of the composite, but it can be extremely time and resource consuming as it requires specific software and hardware for image acquisition and processing, and material to be analysed.

This paper presents a new algorithm to generate a random distribution of fibres that does not suffer from the above mentioned problems. A statistical analysis is performed on the generated arrangements to demonstrate their correspondence to random distributions of reinforcements. The inter-ply matrix-rich areas are not considered in this study. A mechanical analysis demonstrates that the transversal isotropy typical of these materials is fully captured.

## 2. Statistical spatial descriptors

In order to quantitatively characterise the spatial distribution of fibres generated by any given algorithm, different statistical functions can be used.

### 2.1. Voronoi polygon areas

A Dirichlet tessellation is defined as a subdivision of a region [15], determined by a set of points, where each point has associated with it a sub-region that is closer to it than to any other. These sub-regions are named Voronoi polygons. The standard deviation of the areas of the Voronoi polygons defines the more or less periodic distribution of fibres – in a periodic distribution all Voronoi polygons are equal, hence the standard deviation of the areas is zero.

### 2.2. Neighbouring fibre distances

Using the concept of Voronoi polygons, it is possible to calculate the standard deviation of the average of the distances between one given fibre and its neighbouring fibres. A neighbouring fibre is one that shares a side of the Voronoi polygon with the fibre of interest. This measure provides information on how separate from each other the fibres are. Like the standard deviation of the areas of Voronoi polygons, a value of zero corresponds to a periodic distribution.

### 2.3. Nearest neighbour distances

This measure can be obtained easily as the Probability Density Function (PDF) of the distance from one given fibre to its nearest one. Identically, 2nd nearest and 3rd nearest neighbour distances can be computed. The resulting PDFs provide information on the short distance fibre interaction. This function is also sensitive to point clustering. If the PDF plot of the nearest neighbour distances shows a peak for a specific distance followed by a steep decrease, this is an indication that the fibres could be clustered. However, if the 2nd and 3rd neighbour distances show a smooth decrease, then this indicates that there is no clustering but, because of the high fibre volume fraction, the nearest neighbour distance is very close to a peak – the more fibres there are in the RVE, the more packed they have to be for them all to fit in. It is important that this characteristic is well reproduced since experience shows that damage initiation is likely to occur in regions where the fibres are closer together [3].

### 2.4. Nearest neighbour orientation

Using the information about the nearest fibre position determined in the previous statistical spatial descriptor, the orientation at which the nearest fibre is positioned can be determined and studied. This descriptor is given by a Cumulative Distribution Function (CDF) which represents the total number of fibres that have the nearest neighbour oriented along a certain direction, measured clockwise with respect to the horizontal axis. This CDF is normalised with respect to the total number of fibres. The CDF representation for a perfectly random distribution of inclusions is a straight diagonal line meaning that a given orientation has the same probability of occurring as any other orientation. Deviations from this line will be visible if there is a preferred orientation on the fibre spatial arrangement as is the case of periodic distributions.

### 2.5. Ripley's K function

Ripley's $K$ function, also known as the second order intensity function, has been demonstrated to be one of the most informative descriptors of spatial patterns by Pyrz [6]. Unlike the nearest neighbour functions which analyse short range interaction between the fibres, Ripley's $K$ function $(K(h))$ provides insight about the pattern at several distances. $K(h)$ can be defined as the ratio between the number of extra points expected to lie within a radial distance $h$ of an arbitrary point, and the number of points per unit area. $K(h)$ can be estimated by (already accounting for edge effects) [16]:

$$\widehat{K}(h) = \frac{A}{N^2} \sum_i \sum_{j \neq i} \frac{I(d_{ij} \leqslant h)}{w(l_i, l_j)} \tag{1}$$

where $A$ is the area of the region, $N$ is the total number of fibres, $d_{ij}$ is the distance between points $i$ and $j$, and $I(\,)$ is an indicator function having the value 1 if the condition between brackets holds true and the value 0 if the condition is false. $w(l_i, l_j)$ is a weight function having the value 1 if the circle with centre at point $l_i$ and radius $d_{ij}$, i.e., passing by point $l_j$, is completely inside the area of study. If not, $w(l_i, l_j)$ is the proportion of the circumference of that circle lying in the study area. Ripley's $K$ function for the Poisson point pattern, $K_P(h)$, is given by

$$K_P(h) = \pi h^2 \quad h > 0 \tag{2}$$

If the plot of $\widehat{K}(h)$ is below the Poisson curve, $K_P(h)$, then there likely is some degree of regularity on the distribution. If, on the other hand, $\widehat{K}(h)$ is above the Poisson curve, the distribution is exhibiting clustering. A stair-shaped plot of $\widehat{K}(h)$ is an indication of a periodic pattern like a square or an hexagonal distribution of fibres.

The functions given by Eqs. (1) and (2) can be compared using (3)

$$\widehat{L}(h) = \sqrt{\frac{\widehat{K}(h)}{\pi}} - h \tag{3}$$

Peaks of positive values in a plot of $\widehat{L}(h)$ would indicate clustering while negative troughs indicate regularity, for the corresponding distance $h$.

### 2.6. Pair distribution function

The pair distribution function, $g(h)$, is defined as the probability of finding the centre of a fibre inside an annulus of internal radius $h$ and thickness $dh$ with centre at a randomly selected fibre. The concept can be defined by [5]

$$g(h) = \frac{1}{2\pi h \rho dh} \frac{1}{N} \sum_{i=1}^{N} n_i(h) \tag{4}$$

While Ripley's $K$ function can distinguish between different patterns, $g(h)$ describes the intensity of fibre distances. For a periodic pattern, for example, the plot of $g(h)$ shows sharp peaks corresponding to the distances between the periodically arranged fibres. In a Poisson point distribution, the complete randomness of the fibre distribution will assure that $g(h) = 1$ for all distances considered. A statistically valid fibre distribution will have $g(h)$ tending to 1 when the distance $h$ increases.

## 3. Description of algorithm to generate a RVE

In order to overcome the difficulty in generating time-effectively an RVE with a high fibre volume fraction, a new algorithm was developed. Following Trias' conclusions [17], a value of $50 \times R$ is chosen for the RVEs dimension ($\delta = 50$).

The algorithm is called `RAND_uSTRU_GEN`. Its name derives from *Random Microstructure Generator*. The flowchart of this algorithm is presented in Fig. 1. Each iteration of the algorithm is composed of three steps. By the end of an iteration, the current fibre volume fraction, $v_f^{cur}$, is compared to the fibre volume fraction requested at the beginning of the algorithm by the user, $v_f^{req}$. If $v_f^{cur}$ is greater or equal than $v_f^{req}$, the algorithm stops and outputs the results. If the condition is not yet verified, then the algorithm moves on to the next iteration until the condition is satisfied. Since the algorithm is destined to generate fibre distributions to be used in micromechanical finite element analysis, a condition of material periodicity has been imposed along opposite edges of the RVE. A minimum distance between fibres is also imposed to inhibit areas of poor mesh quality between the fibres.

The following subsections describe what takes place inside each of the three steps of the algorithm.

### 3.1. STEP 1 – Hard-core model

The first step of the algorithm is based upon the classical hard-core model. For every position of fibre centre generated, a compatibility check is performed; if the new position does not overlap with any of the existing fibres, the new position is accepted; otherwise, it is discarded. A new check to see if $v_f^{req}$ has been achieved is performed and if so, the results are outputted. Only 50,000 attempts at fibre placement are performed per iteration – this number results from experience showing that more attempts are not likely to provide meaningful improvements.

### 3.2. STEP 2 – Stirring the fibres

Step two can be seen as an heuristic as it helps the algorithm to create matrix-rich areas on the RVE that increase the probability of success of the hard-core model in allocating new fibres. The corresponding flowchart is presented in Fig. 2. Variable $i_f$ is a counter

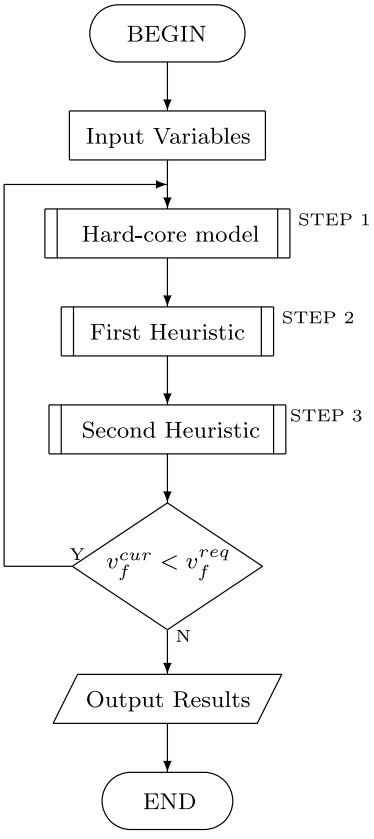


**Fig. 1.** Flowchart of algorithm `RAND_uSTRU_GEN`.

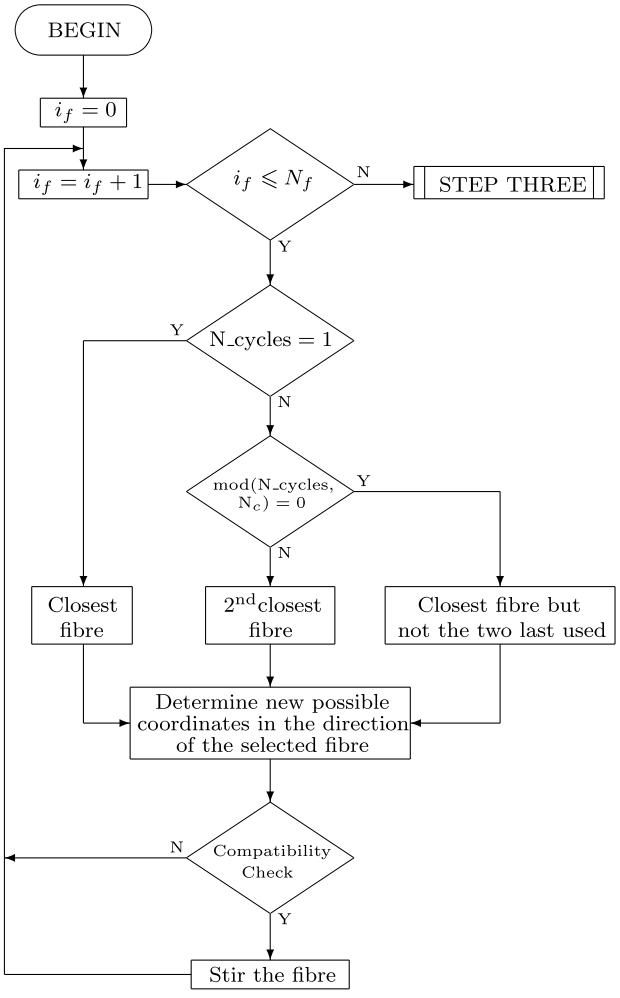


**Fig. 2.** Flowchart of STEP 2 in algorithm `RAND_uSTRU_GEN`.

and $N_f$ the total number of fibres already assigned to the RVE in previous iterations.

The matrix-rich areas are created by stirring the fibres. The small displacements imposed on the fibres are a consequence of searching for one of the closest (*not* necessarily *the* closest) fibres and moving the fibre in that direction. Fig. 3 helps to understand the concept.

Let us consider four fibres – *A*, *B*, *C*, and *D* – positioned as displayed in Fig. 3. For the sake of simplicity, let us also consider that fibres *B*, *C*, and *D* are fixed and so are not affected by this stirring process. $A_0$ represents the starting position of fibre *A*. If the algorithm is in its first iteration, fibre *A* will be displaced in the direction of the closest fibre – fibre *B*, in the present case. The direction of the motion is defined by vector M1 while the length of the displacement is a random number between 0 and $l_{A_0B} - \Delta_{\min}$, being $\Delta_{\min}$ the input variable that defines the minimum distance between any two fibre centres, and $l_{A_0B}$ the distance between fibres *A* and *B*. The final position is denoted by $A_1$.

In the next iteration, the fibre in $A_1$ will be shifted in the direction of the closest fibre, but not considering the last fibre used as a reference. Looking at Fig. 3, the closest fibre to $A_1$ is *B*, but it was also the fibre used as reference in the previous iteration. The reference fibre for the present cycle is thus fibre *C*. Again, M2 defines the direction of the motion while the length of the displacement is defined by a random number between 0 and $l_{A_1C} - \Delta_{\min}$. Excluding the first iteration, where there simply is no previous iteration, this is the standard concept for fibre displacements in step two of the algorithm.

The next iteration is not so simple as the previous two. The input variable $N_c$ controls in how many iterations the stirring criteria is changed. By default, $N_c$ has the value 3 since it was found by experience that it is the optimum value in terms of computational efficiency. This means that every three iterations the algorithm changes the stirring criteria. The third iteration will then apply a displacement to the fibre in $A_2$ and the direction of the movement will be towards the closest fibre, but not considering the previous *two* used as reference. In the current example, fibres *B* and *C* were used as reference in the previous two iterations, respectively, so only fibre *D* can be used as reference for the current iteration. Fibre *A* is thus displaced from $A_2$ to $A_3$. This new criteria only affects iterations which are multiple of the value in the input variable $N_c$ – as per flowchart in Fig. 2. If $N_c$ has the value 3, then only iterations 3, 6, 9, ..., 3*n* are affected.

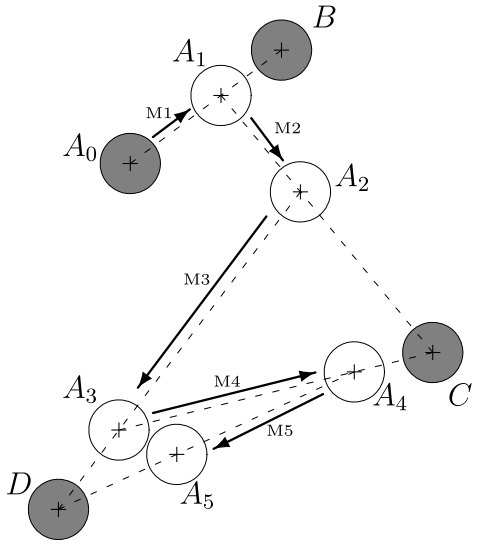


**Fig. 3.** Concept behind STEP 2.

Next cycle will obey to the standard criteria for fibre stirring, i.e., it will look for the closest fibre but not considering the last fibre used as reference for displacement. Therefore, iterations 4 and 5 will cause displacement on fibre *A* from $A_3$ to $A_4$ along M4 towards fibre *C*, and from $A_4$ to $A_5$ along M5 towards fibre *D*, respectively. Iteration 6 is not represented in Fig. 3 but it will use the same criteria as iteration 3 and will move fibre *A* from $A_5$ towards neither fibres *C* nor *D*, but towards fibre *B*.

The example in Fig. 3 does not correspond completely to what really happens during this step since *all* fibres can be stirred and there are many more fibres besides the ones represented as well as new fibres being added every iteration – there can easily be

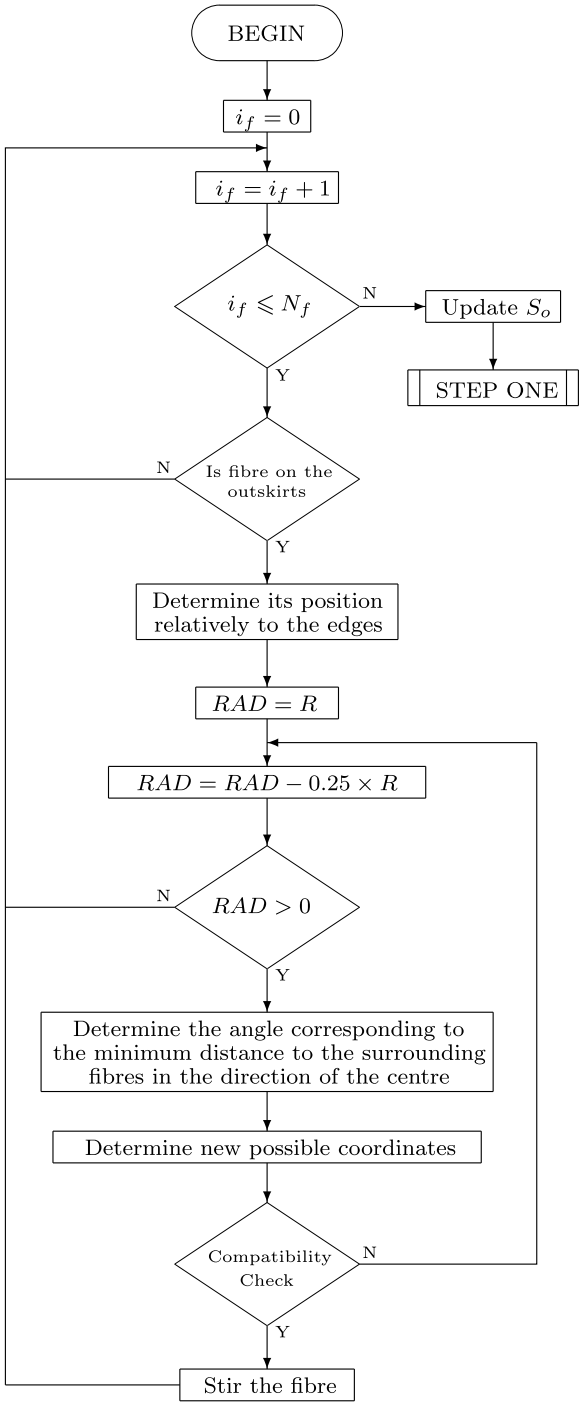


**Fig. 4.** Flowchart of STEP 3 in algorithm `RAND_uSTRU_GEN`.

up to 500 fibres in the RVE. This assures a very dynamic process where very few fibres are left in the same place as they were when the step started.

A compatibility check is performed to guarantee that there is no overlapping of fibres and that the periodicity condition along the edges is maintained.

### 3.3. STEP 3 – Fibres in the outskirts

Step three makes use of a second heuristic. The flowchart of this step is presented in Fig. 4.

The stirring of the fibres positioned in the outskirts will create matrix-rich areas which increase the success rate of fibre positioning during step one. The variables $i_f$ and $N_f$ are defined in the same way as in the previous step. First, it is required to check if the current fibre is on the outskirts of the RVE or not. For this, a definition for the outskirts must be provided. Fig. 5 illustrates the concept.

The variable $S_o$ defines the initial dimension of the square – identified by $B1$ in Fig. 5 – that will be delimiting the outskirts. By default, this variable is set to $3 \times R$. All the fibres with their centres positioned outside square $B1$ will be affected during this step. The outer region of square $B1$ is split in eight different regions. In each region, a different movement will be applied to the fibres in those regions, but always towards the interior of square $B1$, and away from the edges of the RVE. For example, fibres in region 1 will be moved rightwards at an angle between $-\pi/2$ and $\pi/2$ with the horizontal. Regions in the corners of the RVE – regions 5, 6, 7, and 8 – will be stirred away from both edges of the RVE meeting in that corner. For example, fibres in region 5 will be stirred rightwards as well as upwards at an angle between 0 and $\pi/2$.

The stirring lengths can only be $0.75 \times R$, $0.5 \times R$, and $0.25 \times R$. Each possible length is tested for all angles and if it does not comply with the compatibility check for any angle, then the next smaller length is checked. If none of the lengths allows the fibre to be displaced, then the fibre is ignored and it is left where it was. The stirring angles are defined between the limits defined for each region. The exact value is chosen as the one that most reduces the gap to the other fibres.

As the number of iterations increases, the fibres outside square $B1$ will get compacted against each other along the edge of the square, creating a region rich in fibres. In order to avoid this, one other input variable is defined. Variable $S^+$ affects the size of the square defining the outskirts region throughout the consecutive iterations. At the end of each iteration, the size of the square decreases by the value of $S^+$ for each side. Observing Fig. 5, in the first iteration the size of the square is given by $B1$; but in the second iteration will be $B2$, in the third, $B3$, and so on. This alone avoids the clustering of fibres in the outskirts and prevents local variations in the fibre volume fraction.

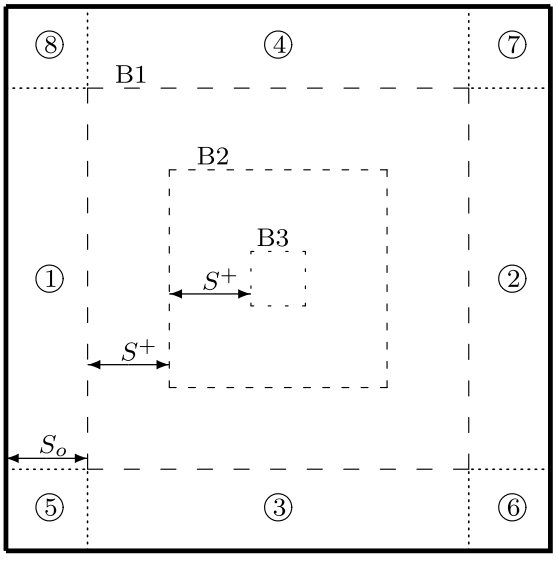


**Fig. 5.** Definition of the outskirts in STEP 3.

## 4. Statistical characterisation of RAND_uSTRU_GEN

In this section, the statistical analysis tools presented in Section 2 will be used to quantitatively characterise the fibre spatial distribution obtained from the algorithm RAND_uSTRU_GEN. The results will be compared with those obtained using Wongsto and Li's algorithm [11] and with two periodic distributions. The values used for the input variables are: $R = 0.0026$ mm, $\delta = 50$, $\Delta_{min} = 2.07 \times R$. All runs were performed in a desktop computer with a Pentium IV 3.0 GHz processor, 1 GB of RAM memory and *hyperthreading* turned ON. Wongsto and Li's method was also programmed here based on their description of the algorithm in Ref. [11].

### 4.1. Time

The first analysis performed was on the time required by each algorithm to run. Table 1 resumes the results for different fibre volume fractions. Periodic distributions are not presented here for comparison since those are generated almost instantaneously. Trias' modified RSA algorithm [17] is also presented for comparison.

The values presented are the mean of five runs for each fibre volume fraction. It is clear that RAND_uSTRU_GEN is the fastest of the three. Wongsto's method always needs at least 250 iterations, so the time it takes to finish is approximately the same for all values of $v_f^{req}$. However, if the condition $\delta \geqslant 50$ was relaxed or if the number of fibres reduced, the time all these algorithms would require would decrease considerably.

### 4.2. Voronoi polygon areas and neighbouring distances

For this test, the coefficient of variation will be used instead of the simple standard deviation, defined according to Eq. (5)

$$\rho(x) = \frac{\sigma(x)}{\mu(x)} \tag{5}$$

The variable $x$ represents the areas of the Voronoi polygons or the distances to neighbouring fibres corresponding to the spatial fibre distribution in analysis. Table 2 shows the coefficient of variation of both areas of Voronoi polygons, $\rho_A$, and neighbouring distances, $\rho_D$, for each method. Periodic distributions obviously have $\rho_A = \rho_D = 0$.

**Table 1**
Mean ($\mu$) and standard deviations ($\sigma$) of time in minutes required to run each algorithm

| $v_f^{req}$ | RAND_uSTRU_GEN | | Wongsto and Li [11] | | Trias [17] |
|---|---|---|---|---|---|
| | $\mu$(time) | $\sigma$(time) | $\mu$(time) | $\sigma$(time) | $\mu$(time) |
| 0.45 | 0.03 | 0.01 | 7.23 | 1.27 | 1.67 |
| 0.48 | 0.12 | 0.04 | 6.90 | 0.72 | 2.48 |
| 0.49 | 0.15 | 0.01 | 6.46 | 0.80 | 5.82 |
| 0.51 | 0.28 | 0.05 | 6.92 | 0.77 | 13.56 |
| 0.53 | 0.44 | 0.07 | 6.92 | 0.61 | 22.54 |
| 0.55 | 0.68 | 0.01 | 7.91 | 0.57 | 44.86 |
| 0.57 | 1.04 | 0.08 | 7.26 | 0.77 | 80.17 |
| 0.59 | 1.34 | 0.12 | 7.66 | 0.80 | 127.67 |
| 0.61 | 1.75 | 0.16 | 8.03 | 1.07 | 331.05[a] |
| 0.63 | 2.37 | 0.10 | 7.12 | 0.49 | 615.70[a] |
| 0.65 | 3.31 | 0.16 | 7.20 | 0.45 | 1145.09[a] |

Values marked superscript 'a' were extrapolated.

**Table 2**
Coefficient of variation for Voronoi polygon areas and distances to neighbouring fibres

| 56% | $\rho_A$ | $\rho_D$ |
|---|---|---|
| RAND_uSTRU_GEN | 0.137 | 0.196 |
| Wongsto's method [11] | 0.129 | 0.190 |
| Matsuda's *Y*-distribution [5] | 0.106 | 0.190 |
| Matsuda's point distribution [5] | 0.135 | 0.256 |
| 65% | $\rho_A$ | $\rho_D$ |
| RAND_uSTRU_GEN | 0.099 | 0.170 |
| Wongsto's method [11] | 0.077 | 0.125 |

Two similar tests were performed – one with 56% in $v_f^{req}$ and a second with 65%. The results for 56% are also compared with values from Matsuda et al. [5]. The values presented for RAND_uSTRU_GEN and Wongsto's method are the mean of five runs.

For $v_f^{req}$ of 56% the coefficients of variation of the Voronoi polygon areas are all very close to each other except for Matsuda's *Y*-distribution that presents poorer performance. As for the distance to neighbouring fibres, Matsuda's point distribution provides better results while all others are at the same level. When the fibre volume fraction is increased, the fibres are compacted and the distance that the fibres can be stirred by both methods is decreased. This means that the fibres will have less chance to move around, and for Wongsto's method this has a significant impact since the fibres start from a periodic array and have difficulty abandoning that periodicity. The coefficient of variation for both functions diverge from each other, leaving RAND_uSTRU_GEN with a better performance since it is an almost purely random algorithm for generating fibre spatial distributions.

### 4.3. Ripley's K function

For the next four subsections, two fibre volume fractions are used: 56% and 65%. For each volume fraction, 20 different distributions were generated and analysed. Each curve represents the average value and for each of them, the minimum and maximum values were added as errorbars.

Function $L(h)$, which measures the difference between the $K$ function of a Poisson distribution and the estimate of $K(h)$ of any other distribution, is represented in Fig. 6 for each fibre volume fraction. Fig. 6b in particular shows that Wongsto's method seems to become inconstant, oscillating considerably more than for a lower fibre volume fraction.

The two periodic distributions exhibit a saw-shaped function since the distances between fibres are regularly pre-defined. One interesting aspect is the evolution of $\widehat{K}(r)$ for Wongsto's method for 56% of fibre volume: at short distances, the curve is below $K_P(r)$, while for long distances the curve is above $K_P(r)$ with tendency to diverge from it. This means that for short distances the method exhibits regularity – probably because it starts with a regular pattern – while for long distances the algorithm creates some degree of clustering. RAND_uSTRU_GEN maintains itself parallel and close to the Poisson distribution. For $v_f^{req} = 65\%$, Wongsto's method starts exhibiting a saw-shaped curve, influence of the original hexagonal distribution. On the other hand, RAND_uSTRU_GEN is able to maintain itself parallel and close of the Poisson curve.

### 4.4. Pair distribution function

The pair distribution function is plotted in Fig. 7 for all four fibre distributions and for each fibre volume fraction in analysis.

It clearly shows the peaks normally detected for periodic distributions, but it also shows that both Wongsto's method and RAND_uSTRU_GEN tend to oscillate close to 1, which is the pair distribution function of a perfect Poisson distribution. Increasing the fibre volume fraction does not create any substantial differences.

### 4.5. Nearest neighbours

Figs. 8–10 show the PDFs for the first, second and third nearest neighbours. It can be seen in the figures that the PDF plots for periodic distributions are nothing more than straight peaks, not reproducing the short range interaction of fibres of the bulk material. Increasing the fibre volume fraction leads to a shift in the curves to the left, signalling that the fibres are closer now than before.

Visible in Fig. 8 is the very steep curve of both random distributions. This happens not because of regularity in the distribution, but because the fibres are so densely compacted against each other due to the high fibre volume fraction and the imposed minimum distance $\Delta_{min}$. The same does not happen in Figs. 9 and 10, which show a more smooth decrease in the second and third nearest

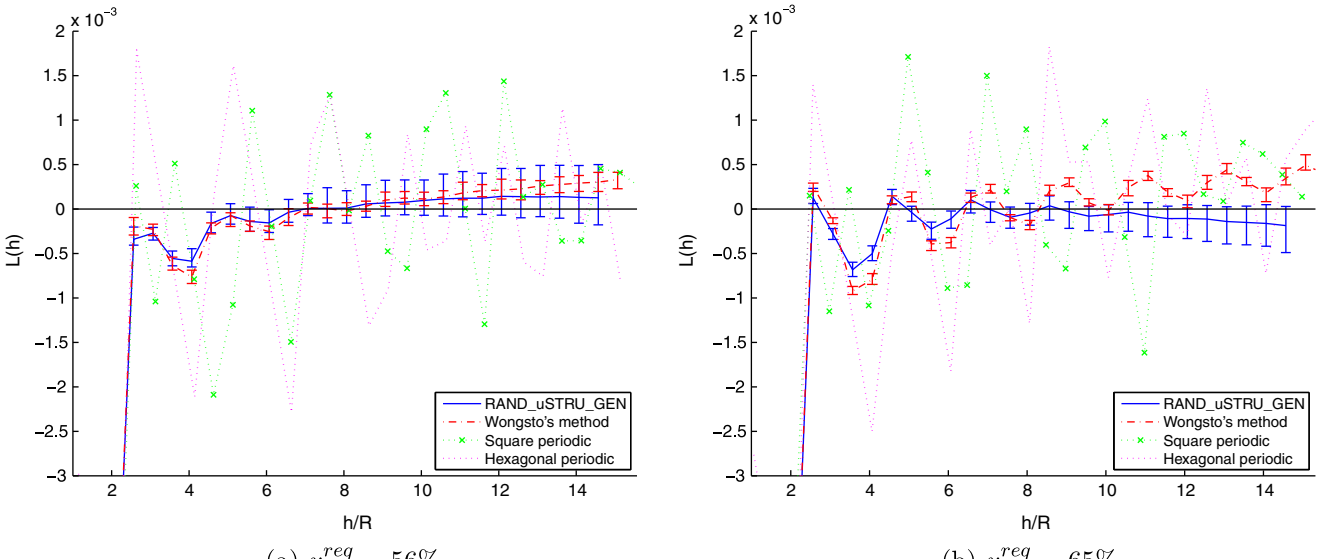


(a) $v_f^{req} = 56\%$ (b) $v_f^{req} = 65\%$

**Fig. 6.** $L(h)$ function for different volume fractions.

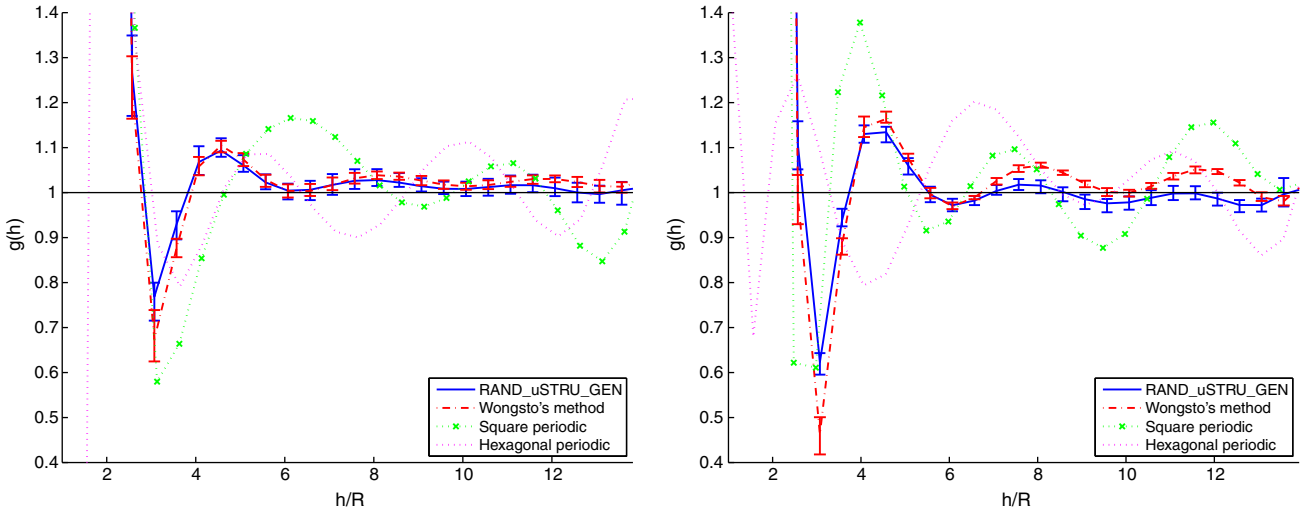


(a) $v_f^{req} = 56\%$ (b) $v_f^{req} = 65\%$

**Fig. 7.** Pair distribution function for different volume fractions.

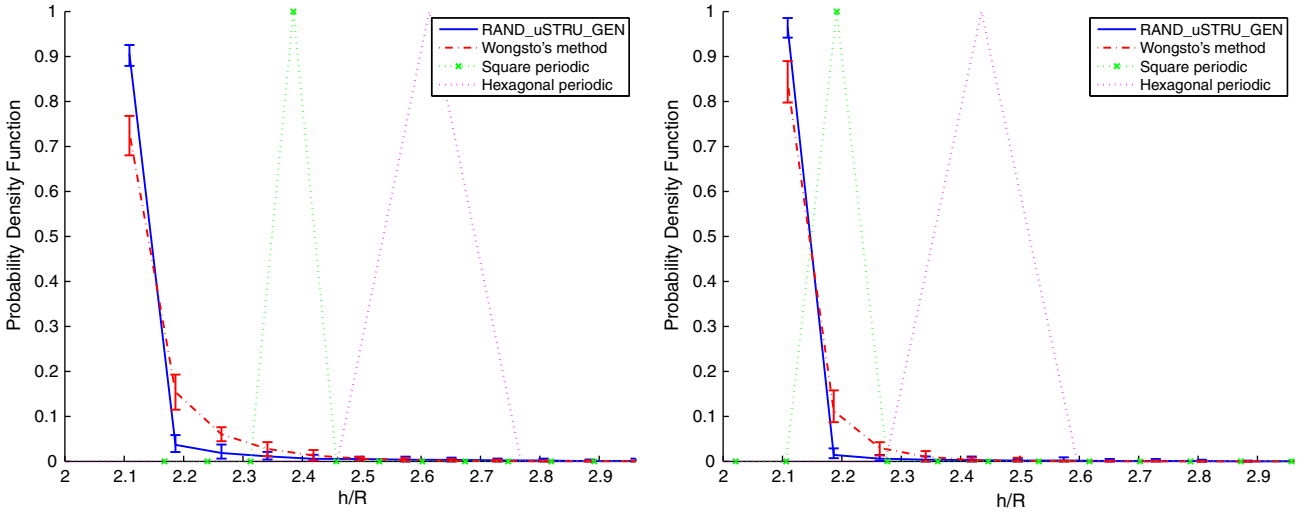


(a) $v_f^{req} = 56\%$ (b) $v_f^{req} = 65\%$

**Fig. 8.** First nearest neighbour function.

neighbour PDFs meaning a lesser denseness on the second and third nearest neighbours throughout the generated distributions.

### 4.6. Nearest neighbour orientations

Fig. 11 shows the cumulative distribution function for the two fibre volume fractions in analysis. It can be seen that the two periodic distributions exhibit preferable orientations of the nearest fibre as indicated by the stair-shaped plots. Both Wongsto's algorithm and `RAND_uSTRU_GEN` perform very well following the Poisson's straight line of cumulated probability.

However, for a fibre volume fraction of 65% it is visible some degree of preference on the orientation of the nearest fibre in Wongsto's algorithm denounced by its stair-shaped plot similar to the hexagonal periodic distribution. This is due to the fibres being too close to each other in an originally hexagonal periodic arrangement and have some difficulty abandoning that original arrangement. `RAND_uSTRU_GEN` maintains its almost perfect random orientation of nearest fibre even for high fibre volume fractions.

## 5. Material characterisation of generated RVE

A very important characteristic of real composites reinforced by unidirectional fibres is the transversal isotropy in the plane perpendicular to the fibre direction for any individual ply in a laminate. It is thus required to verify if the generated random spatial distribution of fibres is able to adequately model this property. Two hundred and fifty fibre spatial distributions with $v_f^{req} = 60\%$ were generated using `RAND_uSTRU_GEN` and two of them are represented in Fig. 12. ABAQUS® [18] software was used to run the finite element analyses.

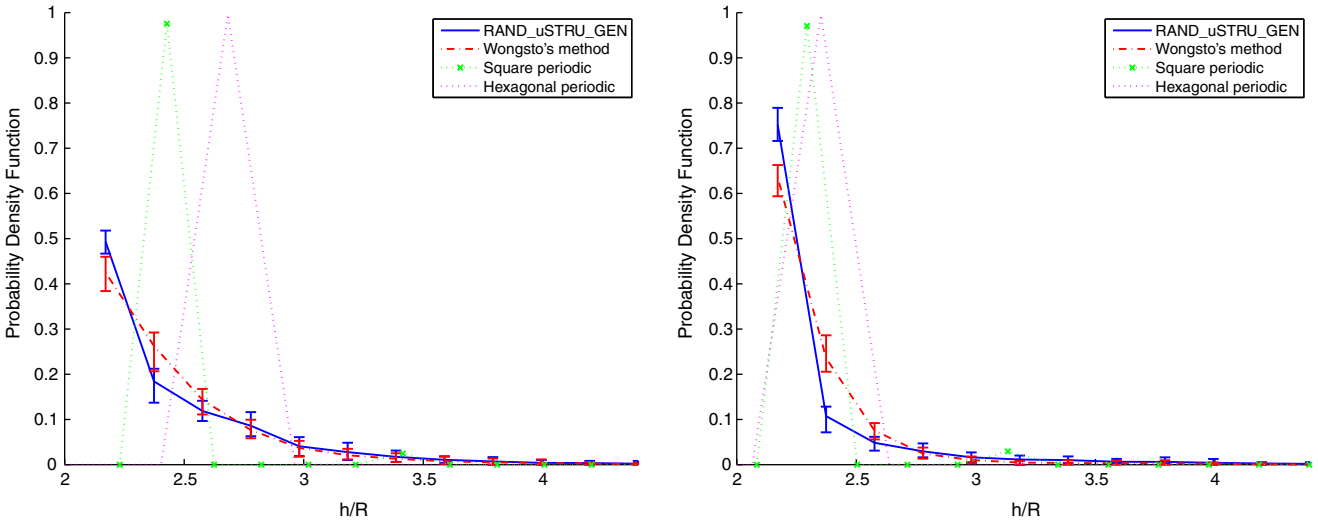


(a) $v_f^{req} = 56\%$ (b) $v_f^{req} = 65\%$

**Fig. 9.** Second nearest neighbour function.

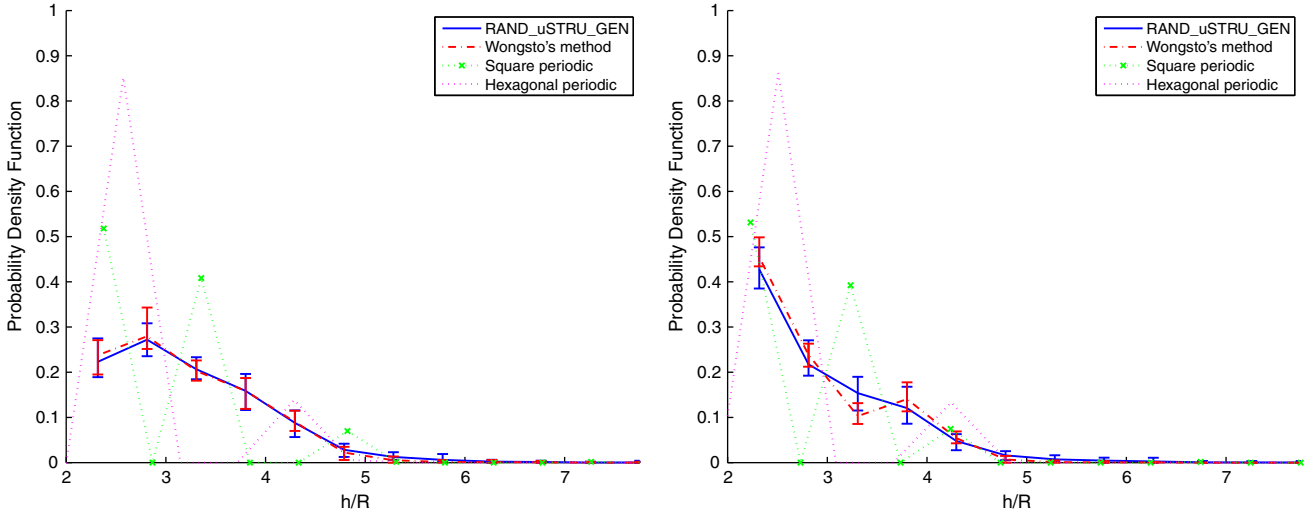


(a) $v_f^{req} = 56\%$ (b) $v_f^{req} = 65\%$

**Fig. 10.** Third nearest neighbour function.

### 5.1. Finite element modelling

One of the material sets considered at the World Wide Failure Exercise [19] was chosen for the analyses – E-glass/MY750/HY917/DY063. Both fibre and matrix are considered isotropic materials. Their elastic properties are summarised in Table 3.

For the analyses, generalised plane strain 3-node linear elements were used from ABAQUS® element library – elements CPEG3. Following Van der Sluis et al. [20], periodic boundary conditions (PBCs) were applied to the RVE. The right and top sides as well as the right-bottom and left-top corners of the RVE have independent degrees of freedom. The left-bottom corner is constrained to prevent rigid body motions. PBCs force the remaining corners and sides to have their displacements related with the former by the following equations:

$$\begin{aligned} \mathbf{u}_B - \mathbf{u}_T + \mathbf{u}_{LT} &= 0 \\ \mathbf{u}_L - \mathbf{u}_R + \mathbf{u}_{RB} &= 0 \\ \mathbf{u}_{RT} - \mathbf{u}_{RB} - \mathbf{u}_{LT} &= 0 \end{aligned} \tag{6}$$

where B, T, L, and R correspond to bottom, top, left, and right edges. When referring to the displacement of a corner, two letters are used corresponding to the edges intersecting on that corner.

By applying different displacement sets to the independent degrees of freedom, one can determine different material properties. $E_2$ and $\nu_{23}$ is determined by applying an horizontal movement to the right side while to determine $E_3$ and $\nu_{32}$ a vertical displacement is applied to the top side. $G_{23}$ is determined by applying horizontal displacement on the top side and a vertical displacement to the right side. The elastic properties were obtained through averaging techniques [21] using the following Eqs. (7):

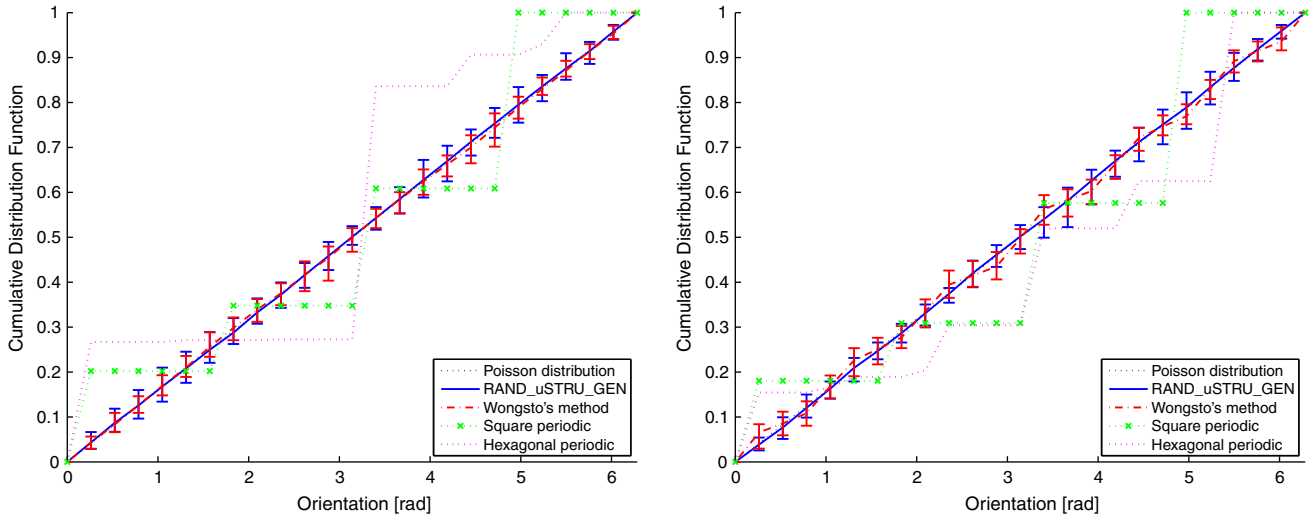


**Fig. 11.** Nearest neighbour orientation function.

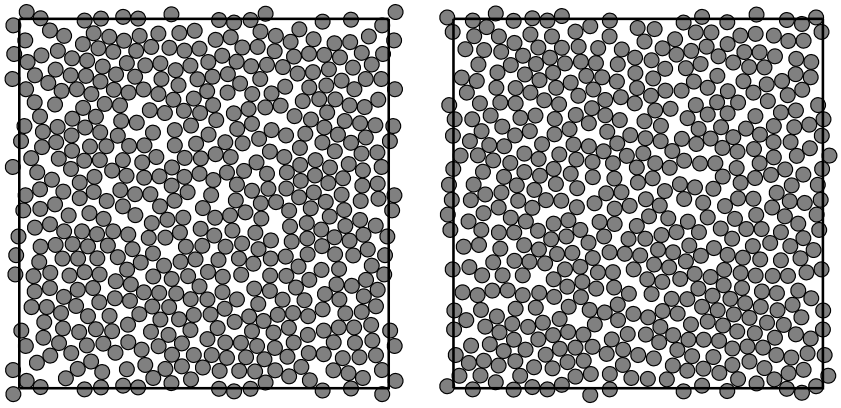

**Fig. 12.** Examples of generated distributions with $v_f^{req} = 60\%$.

**Table 3**
Elastic properties of constituents [19]

| | Fibre | Matrix |
|---|---|---|
| Young's modulus (GPa) | 74 | 3.35 |
| Poisson's ratio | 0.2 | 0.35 |

$$E_k = \frac{\sum_{i=1}^{N} \sigma_{kk}^i A^i}{\sum_{i=1}^{N} \varepsilon_{kk}^i A^i} \quad \nu_{jk} = -\frac{\sum_{i=1}^{N} \varepsilon_{kk}^i A^i}{\sum_{i=1}^{N} \varepsilon_{jj}^i A^i} \quad G_{23} = \frac{\sum_{i=1}^{N} \sigma_{23}^i A^i}{\sum_{i=1}^{N} \varepsilon_{23}^i A^i} \tag{7}$$

where $N$ is the total number of integration points considered, $\sigma_{kk}^i$ and $\varepsilon_{kk}^i$, respectively represent the $k$-component of stress and strain calculated in the integration point of each element and $A^i$ is the area of that element.

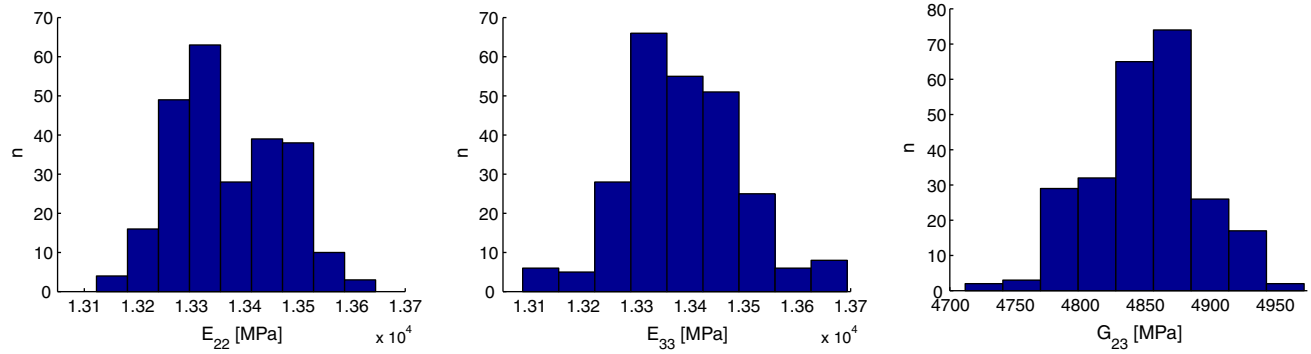


**Fig. 13.** Young's moduli and transverse shear modulus.

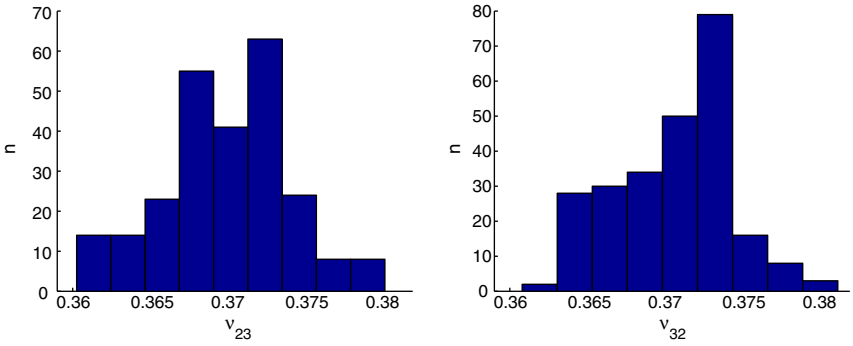


**Fig. 14.** Poisson's ratios.

**Table 4**
Calculated effective properties

| | $E_2$ (MPa) | $E_3$ (MPa) | $\nu_{23}$ | $\nu_{32}$ | $G_{23}$ (MPa) | $G_{23}^{calc}$[a] (MPa) |
|---|---|---|---|---|---|---|
| Mean | 13,367 | 13,387 | 0.370 | 0.371 | 4851 | 4878 |
| Standard deviation | 101 | 113 | 0.004 | 0.004 | 43 | – |
| Experimental [19] | 16,200 | 16,200 | 0.400 | 0.400 | 5786[a] | 5786 |
| Error (%) | 17.5 | 17.4 | 7.5 | 7.3 | 16.2 | – |

[a] Values calculated assuming transversal isotropy.

**Table 5**
Proof of transverse isotropy

| | $\frac{E_2\nu_{32}}{E_3\nu_{23}}$ | $\frac{E_2}{E_3}$ | $\frac{\nu_{23}}{\nu_{32}}$ | $\frac{G_{23}^{calc}}{G_{23}}$ |
|---|---|---|---|---|
| Mean values | 1.000 | 0.999 | 0.999 | 1.006 |

### 5.2. Analyses and results

A total of 250 distributions were generated and the transverse material properties computed for each of them. Figs. 13 and 14 present the results in histogram format. Table 4 provides a summary of these analysis.

The well known relation shown in Eq. (8) between the two Young's moduli and Poisson's ratios allows to better compare these results.

$$\frac{\nu_{23}}{E_2} = \frac{\nu_{32}}{E_3} \iff \frac{E_2\nu_{32}}{E_3\nu_{23}} = 1 \tag{8}$$

The transversal isotropy can also be described by $E_2 = E_3$, $\nu_{23} = \nu_{32}$ and $G_{23} = \frac{E_2}{2(1+\nu_{23})}$. Table 5 provides the results of applying these equations and Eq. (8) to the calculated values in Table 4. It can be seen that all values are very close to 1 in all ratios. It can thus be concluded that the generated random spatial distributions of fibres respect the transversal isotropy of the material in the perpendicular plane to the fibre direction.

## 6. Conclusions

A new algorithm to generate random spatial distributions of fibres has been proposed. The algorithm is able to generate random distributions for high values of fibre volume fractions in a short amount of time by making use of two heuristics specially developed. The algorithm gives the user a high level of control through the several input variables it requires.

The generated distributions were analysed using statistical functions and descriptors and the algorithm's performance was compared with the completely spatial randomness of a Poisson distribution. A good agreement was found in all statistics analysed.

A numerical study to demonstrate that the generated fibre distributions were able to represent the transversal isotropy of the material was performed. A good agreement between independently calculated material properties in different loading schemes was found to exist.

It can therefore be concluded that the new algorithm is able to adequately generate a random fibre distribution that is materially and statistically equivalent to that of randomly distributed long-fibre reinforced materials. The algorithm can be effectively used as the basis for the definition of micromechanical finite element models, and for the investigation of the inelastic response of the constituents of composite materials.

## Acknowledgements

The financial support of the Portuguese Foundation for Science and Technology (FCT) under the PhD scholarship SFRH/BD/24045/2005 and under the project PDCT/EME_PME/64984/2006 is acknowledged.

## References

[1] Shan Z, Gokhale AM. Representative volume element for non-uniform microstructure. Comput Mater Sci 2002;24(3):361–79.
[2] Trias D, Costa J, Turon A, Hurtado J. Determination of the critical size of a statistical representative volume element (SRVE) for carbon reinforced polymers. Acta Mater 2006;54(13):3471–84.
[3] Brockenbrough JR, Suresh S, Wienecke HA. Deformation of metal–matrix composites with continuous fibers: geometrical effects of fiber distribution and shape. Acta Metall Mater 1991;39(5):735–52.
[4] Pyrz R. Correlation of microstructure variability and local stress field in two-phase materials. Mater Sci Eng A 1994;177(1–2):253–9.
[5] Matsuda T, Ohno N, Tanaka H, Shimizu T. Effects of fibre distribution on elastic–viscoplastic behaviour of long fibre-reinforced laminates. Int. J. Mech. Sci. 2003;45(10):1583–98.
[6] Pyrz R. Quantitative description of the microstructure of composites. Part I: morphology of unidirectional composite systems. Compos Sci Technol 1994;50(2):197–208.
[7] Buryachenko VA, Pagano NJ, Kim RY, Spowart JE. Quantitative description and numerical simulation of random microstructures of composites and their effective elastic moduli. Int J Solids Struct 2003;40(1):47–72.
[8] Feder J. Random sequential adsorption. J Theoret Biol 1980;87(2):237–54.
[9] Segurado J, Llorca J. A numerical approximation to the elastic properties of sphere-reinforced composites. J Mech Phys Solids 2002;50(10):2107–21.
[10] Wang J-S. Random sequential adsorption series expansion and Monte Carlo simulation. Phys A: Stat Theoret Phys 1998;254(1–2):179–84.
[11] Wongsto A, Li S. Micromechanical finite element analysis of unidirectional fibre-reinforced composites with fibres distributed at random over the transverse cross-section. Composites: Part A 2005;36(9):1246–66.
[12] Jodrey WS, Tory EM. Computer simulation of close random packing of equal spheres. Phys Rev A 1985;32(4):2347.
[13] Oh JH, Jin KK, Ha SK. Interfacial strain distribution of a unidirectional composite with randomly distributed fibers under transverse loading. J Compos Mater 2006;40(9):759–78.
[14] Yang S, Tewari A, Gokhale AM. Modeling of non-uniform spatial arrangement of fibers in a ceramic matrix composite. Acta Mater 1997;45(7):3059–69.

[15] Bowyer A. Computing Dirichlet tessellations. Comput J 1981;24(2):162–6.
[16] Dixon PM. Ripley's *K* function. In: El-Shaarawi WWP Abdel H, editor. Encyclopedia of Environmetrics, vol. 3. John Wiley & Sons, Ltd.; 2002. p. 1796–803.
[17] D. Trias, Analysis and simulation of transverse random fracture of long fibre reinforced composites, PhD thesis, University of Girona, 2005.
[18] ABAQUS® 6.6/Standard User's Manual, Hibbit, Karlsson & Sorensen, Inc., 2006.
[19] Soden P, Hinton M, Kaddour A. Lamina properties lay-up configurations and loading conditions for a range of fibre-reinforced composites laminates. Compos Sci Technol 1998;58(7):1225–54.
[20] van der Sluis O, Schreurs PJG, Brekelmans WAM, Meijer HEH. Overall behaviour of heterogeneous elastoviscoplastic materials: effect of microstructural modelling. Mech Mater 2000;32(8):449–62.
[21] Trias D, Costa J, Mayugo JA, Hurtado JE. Random models versus periodic models for fibre reinforced composites. Comput Mater Sci 2006;38(2):316–24.